AD-A132 684 TEARING INSTABILITY IN AN ANISOTROPIC NEUTRAL SHEET(U) 1/1
NAVAL RESEARCH LAB WASHINGTON DC J CHEN ET AL.
07 SEP 83 NRL-MEMO-5178

UNCLASSIFIED F/G 20/9 NL

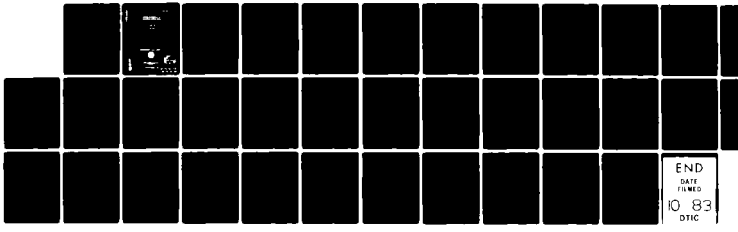

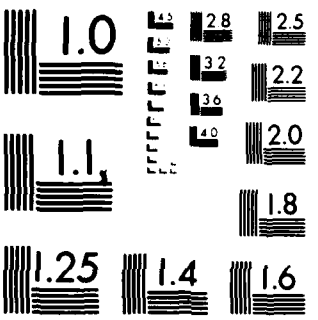

MICROCOPY RESOLUTION TEST CHART
NATIONAL BUREAU OF STANDARDS 1963-A

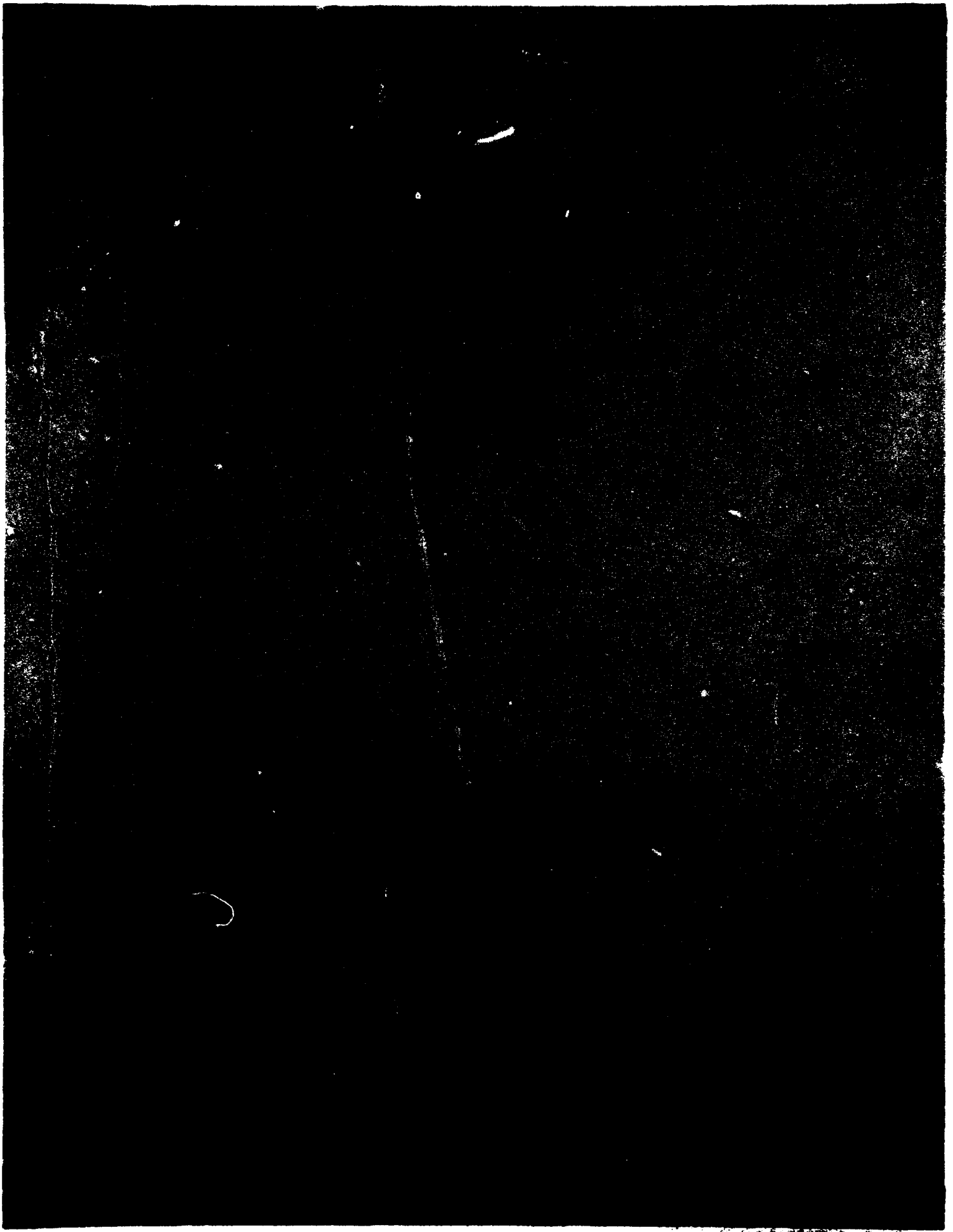

SECURITY CLASSIFICATION OF THIS PAGE (When Data Entered)

REPORT DOCUMENTATION PAGE

READ INSTRUCTIONS BEFORE COMPLETING FORM

1. REPORT NUMBER NRL Memorandum Report 5178	2. GOVT ACCESSION NO. A132684
3. RECIPIENT'S CATALOG NUMBER	
4. TITLE (and Subtitle) TEARING INSTABILITY IN AN ANISOTROPIC NEUTRAL SHEET	5. TYPE OF REPORT & PERIOD COVERED Interim report on a continuing NRL problem.
	6. PERFORMING ORG. REPORT NUMBER
7. AUTHOR(s) J. Chen* and P. Palmadesso	8. CONTRACT OR GRANT NUMBER(s)
9. PERFORMING ORGANIZATION NAME AND ADDRESS Naval Research Laboratory Washington, DC 20375	10. PROGRAM ELEMENT, PROJECT, TASK AREA & WORK UNIT NUMBERS 61153N; RR033-02-44; 47-0884-0-3; NASA 14365
11. CONTROLLING OFFICE NAME AND ADDRESS Office of Naval Research, Arlington, VA 22203 National Aeronautics and Space Admin., Washington, DC 20546	12. REPORT DATE September 7, 1983 13. NUMBER OF PAGES 37
14. MONITORING AGENCY NAME & ADDRESS(if different from Controlling Office)	15. SECURITY CLASS (of this report) UNCLASSIFIED 15a. DECLASSIFICATION DOWNGRADING SCHEDULE

16. DISTRIBUTION STATEMENT (of this Report)

Approved for public release; distribution unlimited.

17. DISTRIBUTION STATEMENT (of the abstract entered in Block 20, if different from Report)

18. SUPPLEMENTARY NOTES

*Present address: Science Applications, Inc., McLean, VA 22102

This research was supported by the Office of Naval Research and the National Aeronautics and Space Administration.

19. KEY WORDS (Continue on reverse side if necessary and identify by block number)

Tearing instability
Anisotropic neutral sheet
Kinetic instability

20. ABSTRACT (Continue on reverse side if necessary and identify by block number)

A study is made of the collisionless tearing-mode stability properties of a field-reversed plasma layer whose temperature distribution is anisotropic. The plasma is confined by its self magnetic field with no external field. A kinetic description is used for both ions and electrons. The wavevector $\underline{k}$ of the perturbation is taken to be parallel to the equilibrium magnetic field $\underline{B}_o$ and perpendicular to the equilibrium current $\underline{J}_o$. The analysis is carried out for the low-frequency perturbation ($|\omega| \ll$

(Continues)

DD FORM 1 JAN 73 1473 EDITION OF 1 NOV 65 IS OBSOLETE
S/N 0102-014-6601

SECURITY CLASSIFICATION OF THIS PAGE (When Data Entered)

20. ABSTRACT (Continued)

ω_{ci}) using simplified particle orbits. The effects of the axis-crossing and nonaxis-crossing orbits are discussed. It is found that the conventional technique of matching the inner and outer asymptotic solutions at the electron inner region is inadequate for the anisotropic case. An intermediate region in which the axis-crossing ion orbits are important is identified. The eigenvalue equation is solved using both analytic approximations and numerical methods to obtain the eigenmode structure and the linear dispersion relation. It is found that the collisionless tearing-mode growth rate is significantly enhanced for $T_\perp > T_\parallel$ and that the mode is strongly stabilized for $T_\perp < T_\parallel$, showing that the anisotropic tearing-mode dominates the conventional isotropic tearing-mode instability.

CONTENTS

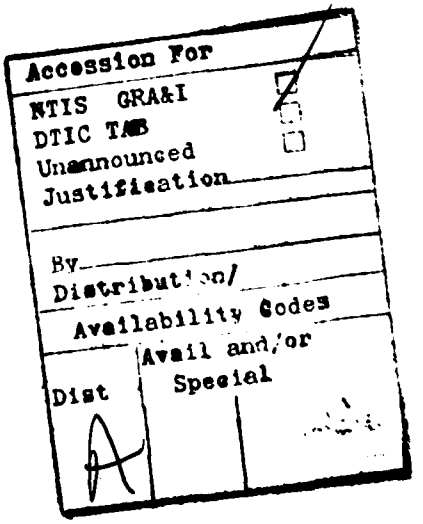

TEARING INSTABILITY IN AN ANISOTROPIC NEUTRAL SHEET

I. INTRODUCTION

In this paper, we investigate the tearing-mode stability properties of a field-reversed plasma layer whose temperature distribution is anisotropic ($T_\perp \neq T_\parallel$). The symbols $\perp$ and $\parallel$ refer to directions perpendicular and parallel to the equilibrium magnetic field, respectively. Figure 1 shows a schematic drawing of the geometry and the coordinate system. The equilibrium magnetic field $\underline{B}_o(z) = B_x^o(z)\hat{\underline{x}}$, indicated by the solid lines, is generated self-consistently by the current $\underline{J}_o(z) = J_o(z)\hat{\underline{y}}$ with no external magnetic field. The magnetic field reverses its direction in the plane $z = 0$ and $J_o(z)$ is symmetric in z. Both ions and electrons are assumed to contribute to the equilibrium current. The number density $n_o(z)$ is also shown in the figure. In this one-dimensional equilibrium, all physical quantities depend on z alone. The plasma is assumed to consist of collisionless ions and electrons so that Vlasov equations are used for both species.

It is well-known that inertia of the current carriers can lead to collisionless tearing instability in a system such as the one described above. Considerable work has been done on the basic collisionless tearing-mode properties of the neutral sheet configuration[1-8]. An example of physical systems that may be modelled by this configuration is the earth's magnetotail[9]. Subsequent to the early work, tearing-mode results have been considered in connection with the magnetotail[10,11]. In these studies, the neutral sheets are generally assumed to have isotropic temperature distributions ($T_\perp = T_\parallel$). However, in a collisionless plasma, the motion of particles parallel to the magnetic field is decoupled from the perpendicular motion and temperature anisotropy can be maintained even in thermal equilibrium. Laval and Pellat[12] used an energy principle analysis to show that collisionless tearing-mode properties can be strongly modified by weak temperature anisotropy. In particular, it was found that the $\underline{k} \parallel \underline{B}_o$ mode can be stabilized by a very small degree of electron temperature anisotropy: $T_{e\perp}/T_{e\parallel} < (1-a_e/\delta)$ where a_e is the electron gyroradius and δ is the layer half-thickness. In this work, neither the dispersion relation nor the marginal condition for the anisotropic case was given. Recently, Chen and Davidson[13] carried out a Vlasov-fluid analysis of a field-reversed ion layer at marginal stability using approximate

Manuscript approved July 14, 1983.

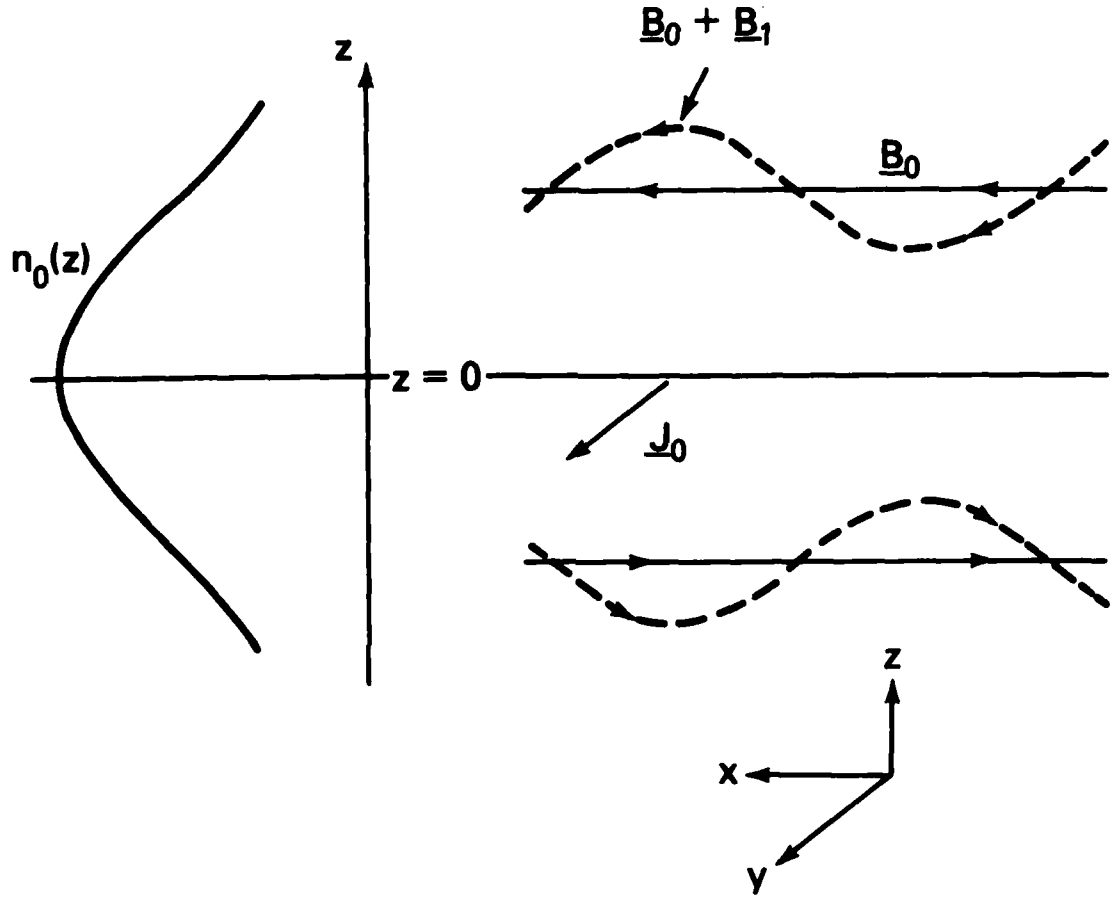

Fig. 1 Schematic drawing of a neutral sheet and the coordinate system. The magnetic field $\underline{B}_0(z)$ reverses direction at z = 0. The dashed lines indicate the magnetic field configuration including the perturbation.

orbits in a cylindrical coordinate system. It was found that relatively small temperature anisotropy in ions significantly modified the stability boundaries. Consistent with the results of Ref. 12, the range of unstable wavenumbers is reduced for $T_{i\perp}/T_{i\parallel} < 1$ and is increased for $T_{i\perp}/T_{i\parallel} > 1$. More recently, Basu and Coppi[14] studied a fluid-like "field swelling" instability in an anisotropic plasma in which the magnetic pressure is comparable to the particle pressure and in which there is no equilibrium current. This analysis is local and is based on the fluid equations. However, in the neutral sheet configuration, the instability is intrinsically nonlocal and the plasma β is much greater than unity in the field-null region so that the fluid equations are invalid. Thus, the treatment of Ref. 14 is not applicable to the tearing-mode instability which is due to resonant particles crossing the field-null region.

A difficulty in treating the neutral sheet configuration is the complicated particle orbits[15]. In order to make the problem tractable analytically, "straight-line" approximations have often been used[8,10] for the particle orbits crossing the null plane. Numerically, the problem is also difficult. In a noteworthy but rarely referenced work, Holdren[16] utilized an integrodifferential equation formalism to show the feasibility to treat the various orbits exactly. In order to minimize the numerical errors, relativistic electrons with large orbits were used and no definitive comparison can be made between the relativistic numerical results and the previous nonrelativistic, approximate results[5]. In addition, the numerics required are prohibitive and it is in general difficult to use this method.

In the present model, we will adopt the straight-line orbits but improve the treatment of the ion orbits. The effects of the small Larmor radius orbits will also be considered. The anisotropic collisionless tearing-mode analysis is carried out for perturbations of the form $\psi(x,z,t) \equiv \hat{\psi}(z)\exp(ikx-i\omega t)$ where the wavevector $\underline{k}$ is taken to be parallel to the equilibrium magnetic field. In Fig. 1, the dashed lines indicate schematically the magnetic field lines including the mirror-like perturbation given above. As a general remark, the problem treated here is different from that of tearing instabilities in tokamak discharges[18] because the tokamak geometry would have an applied magnetic field in the y-

direction (Fig. 1). This alters the prticle orbits significantly. The configuration studied here is more closely related to certain θ-pinches and ion layers.

In Section II, we present the basic linear analysis of the perturbation. In Section III, simplified particle orbits are used to obtain the eigenvalue equation. This equation is solved to give the linear anisotropic dispersion relation. Section IV discusses the results.

II. FORMULATION

Figure 1 shows a schematic drawing of a neutral sheet. We assume that there is no equilibrium electrostatic field and no bulk motion of the plasma (i.e., $\underline{E} \times \underline{B} = 0$). We consider a class of equilibria described by $f_{oj} = f_{oj}((H_{\perp j} - V_j P_{yj}, H_{\parallel j})$ where $j = e,i$ and $(H_{\perp j}, P_{yj}, H_{\parallel j})$ are the single-particle constants of the motion in the equilibrium magnetic field. Here, $H_{\perp j} = (m_j/2)(v_y^2 + v_z^2)$, $P_{yj} = m_j v_y + (q_j/c)A_y^o(z)$, $H_{\parallel j} = (m_j/2)v_x^2$ and $A_y^o(z)$ is the vector potential for the equilibrium magnetic field, where q_j is the electric charge, m_j is the mass, and V_j = constant is the mean drift velocity of the species j.

A. Linear Eigenvalue Equation

The analysis is carried out for perturbations of the form $\psi(x,z,t) = \hat{\psi}(z)\exp(ikx - i\omega t)$ where the wavevector $\underline{k} = k\underline{\hat{x}}$ is parallel to the equilibrium magnetic field. The magnetic field configuration including this perturbation is indicated by dashed lines in Fig. 1. The characteristic frequency is low with $|\omega| \ll \omega_{ci}$ where $\omega_{ci} = eB_0/m_i c$ is the ion cyclotron frequency in the asymptotic magnetic field $B_o \equiv B_x^o(z = \infty)$. Moreover, we consider the case where $kv_e \sim \omega_{ci}$ which is true for a wide range of parameters of interest so that we also have typically $|\omega| \ll kv_e$, where v_e is the electron thermal velocity. This will be verified a posteriori.

Using the standard method of characteristics, the first-order Vlasov distribution function for each species is

$$f_{1j} = -\frac{q}{m}\int_{-\infty}^{t} dt'(\underline{E}_1 + \frac{1}{c}\underline{v}' \times \underline{B}_1) \cdot \frac{\partial}{\partial \underline{v}'} f_o, \qquad (1)$$

where ($\underline{x}'$, $\underline{v}'$) represents the particle orbits in the equilibrium field with the conditions $\underline{x}'(t' = t) = \underline{x}$, $\underline{v}'(t' = t) = \underline{v}$ and $\psi(t \to -\infty) = 0$ for all perturbation quantities. The time integration is carried out along the unperturbed orbits. In the above equation and in the remainder of the paper, the species index j = e,i is suppressed where no confusion arises. The perturbed fields are given by

$$\underline{B}_1 = \underline{\nabla} \times \underline{A}_1 \ , \tag{2}$$

$$\underline{E}_1 = -\underline{\nabla}\phi - \frac{1}{c}\frac{\partial \underline{A}_1}{\partial t} \ , \tag{3}$$

$$\underline{\nabla} \times \underline{B}_1 = \frac{4\pi}{c}\underline{J}_1 \ , \tag{4}$$

and

$$\underline{\nabla} \cdot \underline{E}_1 = 4\pi\rho_1, \tag{5}$$

where $\underline{A}_1$ and ϕ are the perturbed vector and scalar potentials. In this paper, we choose the Coulomb gauge ($\underline{\nabla} \cdot \underline{A}_o = 0$). Because the characteristic frequency of the perturbation is low, $\omega << \omega_{ci}$, we assume charge neutrality to first order. Note that $B_{1y}(x,z,t) = 0$ for the mirror-like perturbations so that $\underline{J}_1 = J_{1y}(x,z,t)\hat{\underline{y}}$ and $\underline{A}_1 = \psi(x,z,t)\hat{\underline{y}}$.

For the general form $f_o = f_o\,(H_\perp - V_j P_y, H_\parallel)$, note that

$$\frac{\partial f_o}{\partial \underline{v}} = m(\underline{v} - V\hat{\underline{y}})\frac{\partial f_o}{\partial H_\perp} + m\left(\frac{\partial f_o}{\partial H_\parallel} - \frac{\partial f_o}{\partial H_\perp}\right) v_x \hat{\underline{x}}.$$

Using Eqs. (2) and (3) in Eq. (1), straightforward calculation yields

$$f_{1j} = q_i \frac{\partial f_o}{\partial H_\perp}\left[(\phi - \beta_j\psi) + i\omega S_y\right] - ikq_i\left(\frac{\partial f_o}{\partial H_\perp} - \frac{\partial f_o}{\partial H_\parallel}\right)v_x S_y, \tag{6}$$

where S_y is the orbit integral along the unperturbed orbits given by

$$S_y \equiv \int_{-\infty}^{t} dt'(\phi - \frac{1}{c} v_y'\psi) \tag{7}$$

and

$$\beta_j \equiv \frac{v_j}{c}$$

is the uniform mean drift velocity normalized to the speed of light c Here, use has been made of $\partial/\partial t \to -i\omega$ and $\partial/\partial x \to ik$. For the isotropic case, the last term in Eq. (6) vanishes and we trivially recover the previous results[8]. For the anisotropic case, estimating v_x by the typical thermal velocity v_{th}, we note that the ratio of the second term to the third term is of the order of $\omega/(kv_{th})$ which makes the last term in Eq. (6) small in comparison with the first two terms for low frequency perturbations except for a very small degree of anisotropy. This means that the marginal state[13] and the growth rate can be significantly modified in comparison with the isotropic case. It is the purpose of this paper to give a quantitative illustration of this point.

Another consequence of the low-frequency nature of the perturbation is that the perturbed scalar potential ϕ is much smaller than $(v_y/c)\psi$[8]. This can be seen by noting that the electric field E_{1x} along the magnetic field is <u>at most</u> comparable to the components perpendicular to the magnetic field, say, E_{1y}. That is to say, $E_{1x} \lesssim E_{1y}$. This implies

$$\phi \lesssim \left(\frac{\omega}{kv_{th}}\right)\left(\frac{v_{th}}{c}\right)\psi.$$

For the low frequency case ($\omega \ll kv_{th}$), ϕ is much less than $(v_y/c)\psi$ where $v_y \sim v_{th}$ for the typical thermal particle. Physically, this is simply a statement of quasi-neutrality at low frequencies. Although it is theoretically straightforward to include ϕ, we will adopt the simplification of neglecting ϕ in comparison with $(v_y/c)\psi$. Then, the approximate perturbed distribution function is

$$f_{1j} = -q\beta \frac{\partial f_o}{\partial H_\perp}\psi + i\omega q \frac{\partial f_o}{\partial H_\perp} S_y - ikq\left(\frac{\partial f_o}{\partial H_\perp} - \frac{\partial f_o}{\partial H_\parallel}\right)v_x S_y, \tag{8}$$

where the orbit integral [Eq. (7)] has been simplified to

$$S_y = -\frac{1}{c}\int_{-\infty}^{t} dt' v_y' \psi. \tag{9}$$

The first term in Eq. (8) is the usual adiabatic term which does not depend on the [illegible] particle orbits. The second term represents the change in

momentum and the third term represents the change in energy of the particles. In particular, $ikqS_y$ is the time-integrated Lorentz force acting on the particles in the x-direction.

B. Anisotropic Plasma Layer in Thermal Equilibrium

In the preceding section, we have described the general theoretical framework appropriate for equilibria of the type $f_{oj}(H_\perp - V_j P_y, H_\parallel)$. To examine the stability properties in detail, we specialize to the case where the plasma layer consists of two species (electrons and ions), both satisfying the two-temperature Maxwellian distribution given by

$$f_{oj} = \frac{\hat{n}_o}{2\pi T_{\perp j}/m_j} \frac{1}{\sqrt{2\pi T_{\parallel j}/m_j}} \exp\left[-\frac{1}{T_{\perp j}}\left(H_{\perp j} - V_j P_{yj}\right)\right] \exp\left(-\frac{1}{T_{\parallel j}} H_{\parallel j}\right), \quad (10)$$

where $H_{\perp j} = (m_j/2)(v_y^2 + v_z^2)$, $P_{yj} = m_j v_j + (q_j/c)A_y^o(z)$, $H_{\parallel j} = (m_j/2)v_x^2$, V_j = constant is the mean velocity of the species j, and $A_y^o(z)$ is the vector potential for the equilibrium magnetic field. As stated before, the electrostatic field is taken to be zero in the frame of the layer.

The equilibrium particle density and magnetic field profiles corresponding to Eq. (10) depend only on the perpendicular temperature and are well-known[17]

$$n_o(z) = \hat{n}_o \operatorname{sech}^2\left(\frac{z}{\delta}\right), \quad (11)$$

and

$$B_x^o(z) = \frac{2cT_\perp/\delta}{e(V_i - V_e)} \tanh\left(\frac{z}{\delta}\right), \quad (12)$$

where δ is the characteristic half-thickness of the plasma layer given by

$$\delta \equiv \left(\frac{c^2 T_\perp}{2\pi \hat{n}_o}\right)^{1/2} \frac{1}{e(V_i - V_e)} . \quad (13)$$

Here, $T_\perp \equiv T_{i\perp} + T_{e\perp}$, and $\hat{n}_o$ is the maximum number density at $z = 0$ for both species. For $z \to \infty$, we have $B_x^o(z \to \infty) = B_o$ with

$$B_o \equiv \sqrt{8\pi \hat{n}_o T_\perp} , \quad (14)$$

where $B_o > 0$ is chosen without loss of generality. This choice implies $(V_i - V_e) > 0$ so that the total current is in the +y-direction, given by

$$\underline{J}_o(z) = e(V_i - V_e)n_o(z)\hat{\underline{y}}. \tag{15}$$

Because of charge neutrality, the equilibrium ion and electron densities are equal. It is easy to show that the zero electrostatic field condition is equivalent to

$$T_{i\perp}V_e + T_{e\perp}V_i = 0. \tag{16}$$

If we denote the gyroradius of the thermal particles by $a_j \equiv v_{j\perp}/\omega_{cj}$ where $v_{j\perp} \equiv \sqrt{2T_{j\perp}/m_j}$ and $\omega_{cj} = eB_o/m_jc$ with B_o given by Eq. (14), then it is easy to show by using Eqs. (13) and (16) that

$$\frac{a_j}{\delta} = \frac{|V_j|}{v_{j\perp}} \tag{17}$$

and

$$\frac{q_jV_j}{cT_{j\perp}} = \frac{2}{B_o\delta}. \tag{18}$$

As a general remark, the equilibrium configuration described above is obtained by balancing the Lorentz force $c^{-1}(\underline{J}_o \times \underline{B}_o)$ with the perpendicular pressure gradient $-(\partial/\partial z)[n_o(z)T_\perp]$.

III. Stability Properties for an Anisotropic Neutral Sheet

A. Model Orbits

In order to determine the stability properties of the system described by Eqs. (10)-(18), the orbit integral S_y [Eq. (9)] must be evaluated. Generally, the orbits in the equilibrium field are complicted.[15] In the previous calculations on the isotropic neutral sheets, "straight-line" orbits[8,10] have been used to evaluate the orbit integral. In these approximations, the neutral sheet is divided into two regions. In the inner region, $|z| \lesssim d_j \sim \sqrt{a_j\delta}$ where the magnetic field is weak, the orbits

are taken to be straight lines across the null-plane ($z = 0$) and reflected from the surfaces at $|z| \simeq d_j$. Thus, v_y is nearly constant in this region. In addition, the perturbed vector potentrial $\psi = A_{1y}$ is assumed to be constant in the inner region (constant-ψ approximation). In the outer region, $|z| \gtrsim d_j$, the particles are assumed to execute nonaxis-crossing small Larmor radius orbits and these orbits are neglected. In particular, in Ref. 8, the dispersion relation is obtained by matching the inner and outer solutions at $z = \sqrt{2a_e\delta}$. This approximation neglects the axis-crossing ion orbits that extend far beyond the electron inner region since $d_i/d_e \sim (m_i/m_e)^{1/4}$. Although the effects of the axis-crossing electrons are greater than those of the axis-crossing ions, the ion effects dominate in the intermediate region $d_e \lesssim |z| \lesssim d_i$, as will be shown in this section. In the isotropic case, it will turn out that the neglect of the intermediate region does not change the dispersion relation substantially. However, in the anisotropic case, the ion orbits in the intermediate region affects the dispersion relation significantly. In the present analysis, we include the three regions (Fig. 2) and define the boundary surfaces at

$$d_e \equiv \sqrt{2a_e\delta} \tag{19}$$

for the electrons and

$$d_i \equiv \sqrt{a_i\delta/2} \tag{20}$$

for the ions, where $a_j = v_{j\perp}/\omega_{cj}$ is the Larmor radius of a thermal particle with $v_{j\perp} = \sqrt{2T_{j\perp}/m_j}$. Physically, d_e is the distance where the local electron Larmor radius $a_e(d_e) \equiv v_{e\perp}/\omega_{ce}(d_e)$ is equal to $d_e/2$. Here, $\omega_{ce}(d_e) = eB_x^o(d_e)/m_e c$. d_i is the distance where the local ion Larmor radius $a_i(d_i) \equiv v_{i\perp}/\omega_{ci}(d_i)$ is equal to d_i. The factor of $\sqrt{2}$ is somewhat arbitrary and is chosen to avoid overestimating the large ion orbits. Moreover, this choice allows the use of the constant-ψ approximation in the region $|z|/\delta \lesssim d_i/\delta \ll 1$.

The orbit integral S_y [Eq. (9)] will now be evaluated for the three regions as shown in Fig. 2. In the respective inner region for each species, the orbits consists of nearly straight segments[8,10] and v_y is

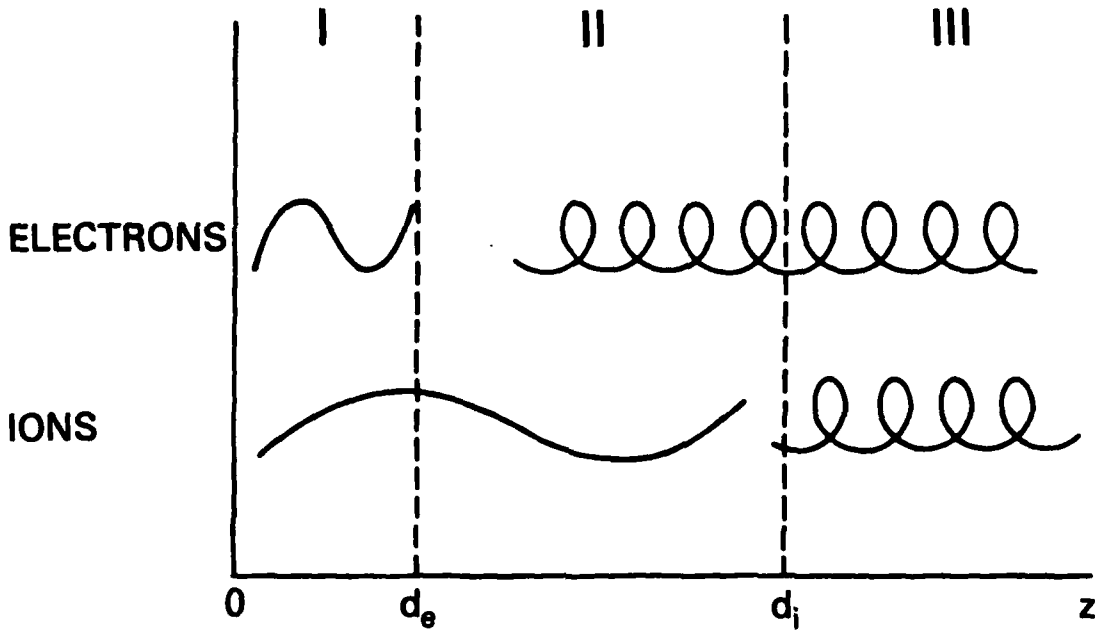

Fig. 2 Schematic drawing of electron and ion orbits.

nearly constant. Then, from Eq. (9), the approximate orbit integral is

$$S_y^{in} = ic^{-1}v_y\ \psi(x,z,t)(kv_x-\omega)^{-1}, \tag{21}$$

where v_x is an exact constant of the motion and the constant-ψ approximation has been used. Using Eq. (21) in the first velocity moment of f_{1j}, we obtain the perturbation current densities for the inner regions (region I for electrons and regions I and II for ions),

$$J_{1i}^{in} = \frac{c}{4\pi\hat{n}_o\delta^2}\frac{2T_{i\perp}}{T_\perp}\left[1 + \left(\frac{\omega}{kv_{i\parallel}}\right)\left(\frac{1}{2}\frac{\delta^2}{a_i^2} + 1\right)Z\left(\frac{\omega}{kv_{i\parallel}}\right)\right.$$
$$\left. - \alpha_i\left(\frac{1}{2}\frac{\delta^2}{a_i^2} + 1\right)W\left(\frac{\omega}{kv_{i\parallel}}\right)\right]n_o(z)\psi\ , \tag{22}$$

and

$$J_{1e}^{in} = \frac{c}{4\pi\hat{n}_o\delta^2}\frac{2T_{e\perp}}{T_\perp}\left[1 + \left(\frac{\omega}{kv_{e\parallel}}\right)\left(\frac{1}{2}\frac{\delta^2}{a_e^2} + 1\right)Z\left(\frac{\omega}{kv_{e\parallel}}\right)\right.$$
$$\left. - \alpha_e\left(\frac{1}{2}\frac{\delta^2}{a_e^2} + 1\right)W\left(\frac{\omega}{kv_{e\parallel}}\right)\right]n_o(z)\psi\ . \tag{23}$$

where the anisotropy parameter is defined by

$$\alpha_j \equiv 1 - \frac{T_{j\perp}}{T_{j\parallel}}\ . \tag{24}$$

The dispersion function is given by

$$Z(\xi) \equiv \frac{1}{\sqrt{\pi}}\int_{-\infty}^{\infty}dx\ \frac{\exp(-x^2)}{x-\xi}$$

and

$$W(\xi) \equiv -\frac{1}{2}Z'(\xi).$$

In deriving Eqs. (22) and (23), use has been made of the equilibrium properties, Eqs. (13), (14), (16) and (18), and $v_{j\parallel} = \sqrt{2T_{j\parallel}/m_j}$.

In the outer regions, regions II and III for electrons and region III for ions, the particles mainly execute $\underline{\nabla B}$ drift motion with the drift

velocity $\underline{V}_D^j$ given by

$$\underline{V}_D^j = - \hat{\underline{y}} \frac{mcv_\perp^2}{2qB_o\delta} \sinh^{-2}\left(\frac{z}{\delta}\right), \tag{25}$$

where $v_\perp^2 \equiv v_y^2 + v_z^2$ is a constant of the motion. This expression is a good approximation for the guiding center motion in the outer regions for most particles ($a_j \ll \delta$) except for the ones with kinetic energy much greater than the thermal energy. Note that, for thermal particles ($v_\perp \approx v_{j\perp}$), $V_D^j/v_{j\perp}$ is of the order of $(a_j/\delta)\sinh^{-2}(z/\delta)$ so that $V_D^j/v_{i\perp}$ is of order unity near $z = d_j$. The actual motion of a particle is then

$$v_y \simeq V_D^j + \breve{v}\cos(\omega_{cj}t + \lambda)$$

and

$$v_z \simeq \breve{v}\sin(\omega_{cj}t + \lambda),$$

where ω_{cj} is the local cyclotron frequency, $\breve{v}$ is the gyration velocity in the V_D frame and λ is the phase angle. Then, the approximate orbit integral S_y for the outer regions is

$$S_y^{out} = ic^{-1}V_D^j(kv_x-\omega)^{-1}\psi - c^{-1}\breve{v}\int_{-\infty}^{t} dt'\cos(\omega_{cj}t' + \lambda)\psi.$$

The second term represents the oscillatory motion in the guiding center frame. Taking the phase average over λ for the low frequency perturbation, it is easy to see that the second term averages to zero and we have

$$S_y^{out} = ic^{-1}V_D^j(kv_x-\omega)^{-1}\psi(x,z,t) \ . \tag{26}$$

Integrating over the velocity space and after some algebra, we obtain

$$J_{1i}^{out} = \frac{c}{4\pi\hat{n}_o\delta^2}\frac{2T_{i\perp}}{T_\perp}\left[1 - \left(\frac{\omega}{kv_{i\parallel}}\right)\frac{Z(\omega/kv_{i\parallel})}{\sinh^2(z/\delta)}\right.$$

$$+ \alpha_i \frac{W(\omega/kv_{i\parallel})}{\sinh^2(z/\delta)}]n_o(z)\psi, \tag{27}$$

and

$$J_{le}^{out} = \frac{c}{4\pi \hat{n}_o \delta^2} \frac{2T_{e\perp}}{T_\perp} [1 - (\frac{\omega}{kv_{e\parallel}}) \frac{Z(\omega/kv_{e\parallel})}{\sinh^2(z/\delta)}$$

$$+ \alpha_e \frac{W(\omega/kv_{e\parallel})}{\sinh^2(z/\delta)}]n_o(z)\psi. \tag{28}$$

In obtaining these expressions, use has been made of the equilibrium relationships Eqs. (17) and (18), and $a_j^2/\delta^2 << 1$ has been dropped.

The third term in the square brackets of each equation is the anisotropy term. In Ref. 8, where the isotropic case is treated, the second term in each equation is neglected by using the ordering $(\omega/kv_{j\parallel}) \sim (a_j/\delta)^{3/2} << 1$ and the ion contribution J_{li}^{in} is neglected in region II. Galeev and Zelenyi[19] estimated the drift velocity by V_D^j [Eq. (25)] without the factor $\sinh^{-2}(z/\delta)$ and concluded that this contribution is small. However, as the discussion following Eq. (25) shows, this term can be of order unity in Eqs. (27) and (38) near $z = d_e$. Moreover, Dobrowolny[8] and Galeev and Zelenyi[19] matched the interior ($|z| < d_e$) and exterior ($|z| > d_i$) solutions at $z = d_e$ by arguing that the interior electron contribution to the perturbed current density [Eq. (23)] is much greater than the external ion contribution [Eq. (27)] for $|z| > d_e$. This argument overlooks the fact that the axis-crossing ion orbits extend far beyond the electron inner region ($|z| = d_e$) so that the relevant comparison in the intermediate region (region II) is between the exterior electrons [Eq. (28)] and interior ions [Eq. (22)]. For the case in which ions and electrons are both anisotropic, the ratio J_{li}^{in}/J_{le}^{out} at $z = d_e$ in region II is approximately $(\alpha_i/\alpha_e)(m_e/m_i)(\delta/a_e)$ which is typicallty of order unity. For the case in which only ions are anisotropic ($\alpha_e = 0$), the ratio is approximately $\alpha_i(\delta/a_e)^{5/2}(m_e/m_i)$ which is much greater than unity. As z increases to d_i, the ratio increases because of the factor $\sinh^{-2}(\bar{z})$ in the electron contribution. Thus, in general, the ion contribution is not negligible in the intermediate region. Moreover, this intermediate region is wider than the electron inner region by a factor of

$d_i/d_e = (T_{i\perp}/T_{e\perp})^{1/4}(m_i/m_e)^{1/4}/2$. For comparable $T_{i\perp}$ and $T_{e\perp}$, this quantity is roughly 4. The intermediate region is in turn thinner than the sheet thickness δ by a factor of $\sqrt{a_i/2\delta} \ll 1$. In this paper, we treat the three-region matching problem (see Fig. 2); in region I, the total current density is $J_{1T} = (J_{1i}^{in} + J_{1e}^{in})$; in region II, $J_{1T} = (J_{1i}^{in} + J_{1e}^{out})$; in region III, the current density is $J_{1T} = (J_{1i}^{out} + J_{1e}^{out})$.

B. Linear Dispersion Relation

The linear eigenvalue equation is obtained by substituting Eqs. (22), (23), (27) and (28) into Eq. (4) according to the three-region scheme described in the preceding section. The equation is then solved subject to the following conditions. The solution ψ must be such that its first derivative $(\partial\psi/\partial z)$ vanishes asymptotically ($|z| \to \infty$) and that the logarithmic derivative is continuous at $|z| = d_e$ and $|z| = d_i$. For the inner region (I), the eigenvalue equation is found to be

$$\frac{d^2\hat{\psi}}{d\bar{z}^2} = \Lambda^2\hat{\psi}(\bar{z}) \tag{29}$$

where $\psi(x,z,t) = \hat{\psi}(z)\exp(ikx-i\omega t)$ and

$$\Lambda^2 \equiv \bar{k}^2 - 2\{1 + \frac{T_{i\perp}}{T_\perp}(\frac{1}{2}\frac{\delta^2}{a_i^2} + 1)[(\frac{\omega}{kv_{i\parallel}})Z(\frac{\omega}{kv_{i\parallel}}) - \alpha_i W(\frac{\omega}{kv_{i\parallel}})]$$
$$+ \frac{T_{e\perp}}{T_\perp}(\frac{1}{2}\frac{\delta^2}{a_e^2} + 1)[(\frac{\omega}{kv_{e\parallel}})Z(\frac{\omega}{kv_{e\parallel}}) - \alpha_e W(\frac{\omega}{kv_{e\parallel}})]\}, \tag{30}$$

with $\mathrm{sech}^2(z/\delta) \simeq 1$ for $|z| < d_e \ll \delta$. Here, $\bar{k} \equiv k\delta$ and $\bar{z} = z/\delta$. By setting $\alpha_i = \alpha_e = 0$, Eqs. (29) and (30) reduce to the inner equation of Ref. 8. In general, Λ is independent of z and the solution is

$$\hat{\psi}^{in}(z) = C\cosh(\Lambda\bar{z}) \tag{31}$$

where C is an integration constant and the symmetric solution has been chosen.

In the intermediate region II, the eigenvalue equation takes on the form

$$\frac{d^2\hat{\psi}}{d\bar{z}^2} = \bar{k}^2\hat{\psi} - 2\{1 + \frac{T_{i\perp}}{T_\perp}(\frac{1}{2}\frac{\delta^2}{a_i^2} + 1)[(\frac{\omega}{kv_{i\parallel}})Z(\frac{\omega}{kv_{i\parallel}}) - \alpha_i W(\frac{\omega}{kv_{i\parallel}})]$$

$$- \frac{2T_{e\perp}}{T_\perp}\left[\left(\frac{\omega}{kv_{e\parallel}}\right)Z\left(\frac{\omega}{kv_{e\parallel}}\right) - \alpha_e W\left(\frac{\omega}{kv_{e\parallel}}\right)\sinh^{-2}(\bar{z})\right]$$

$$\times \operatorname{sech}^2(\bar{z})\hat{\psi}. \tag{32}$$

It is easy to see that the inner ion orbit contribution dominates the small gyroradius electron contribution in this region.

In the exterior region $|z| > d_i$, the orbit of both species are mainly of the small gyroradius drifting type and the eigenvalue equation takes on the form

$$\frac{d^2\hat{\psi}}{d\bar{z}^2} = \left[\bar{k}^2 - 2\operatorname{sech}^2(\bar{z})\right]\hat{\psi} + 2\left\{\frac{T_{i\perp}}{T_\perp}\left[\left(\frac{\omega}{kv_{i\parallel}}\right)Z\left(\frac{\omega}{kv_{i\parallel}}\right) - \alpha_i W\left(\frac{\omega}{kv_{i\parallel}}\right)\right]\right.$$
$$\left. + \frac{T_{e\perp}}{T_\perp}\left[\left(\frac{\omega}{kv_{e\parallel}}\right)Z\left(\frac{\omega}{kv_{e\parallel}}\right) - \alpha_e W\left(\frac{\omega}{kv_{e\parallel}}\right)\right]\right\}\sinh^{-2}(\bar{z})\operatorname{sech}^2(\bar{z})\hat{\psi}. \tag{33}$$

Asymptotically, where the $\underline{\nabla B}$ contribution vanishes due to near uniformity of the equilibrium magnetic field, the solution of the above equation is[20]

$$\hat{\psi}_\infty(z) = D\left(1 + \frac{1}{\bar{k}}\tanh|\bar{z}|\right)\exp\left(-\bar{k}|\bar{z}|\right), \tag{34}$$

where the even solution is chosen and D is an integration constant. As required, the first derivative is proportional to $\exp(-\bar{k}|\bar{z}|)$ and vanishes as $|\bar{z}| \to \infty$.

If we set $\alpha_i = \alpha_e = 0$ in Eq. (30) and match the inner and asymptotic solutions [Eqs. (31) and (34)] at $z = d_e$, then the isotropic results of Ref. 8 are recovered. Equating the logarithmic derivatives of Eqs. (31) and (34) at $z = d_e$, we obtain the linear dispersion relation

$$\Lambda\tanh\left(\Lambda\bar{d}_e\right) = \left(1 + \bar{k}^{-1}\tanh\bar{d}_e\right)\left[\bar{k}^{-1}\operatorname{sech}^2\bar{d}_e - \bar{k}^{-1}\left(1 + \bar{k}^{-1}\tanh\bar{d}_e\right)\right], \tag{35}$$

where Λ is given by Eq. (30) and $\bar{d}_e \equiv d_e/\delta$. This is equivalent to the series representation in terms of generalized Legendre functions given in Ref. 8. Neglecting terms of order $\bar{d}_e \ll 1$, the right hand side can be simplified and we have approximately

$$\Lambda \tanh\left(\Lambda \bar{d}_e\right) = \frac{1}{\bar{k}} - \bar{k}. \tag{36}$$

Using the small-argument expansion of Z function in Eq. (32), we find $\left(\Lambda \bar{d}_e\right) << 1$ for the low-frequency perturbations. Then, keeping only the leading terms in Eq. (36), we find that the instability is primarily due to the resonant electrons and

$$\frac{\gamma}{k v_{e\parallel}} \simeq \left(\frac{a_e}{\delta}\right)^{3/2} \frac{1}{\sqrt{2\pi}} \left(1 + \frac{T_i}{T_e}\right)\left(\frac{1}{\bar{k}} - \bar{k}\right), \tag{37}$$

which is identical to the isotropic result[8]. It shows that $\left(\gamma/k v_{e\parallel}\right) << 1$ scales as $\left(a_e/\delta\right)^{3/2}$ and that $\gamma > 0$ (unstable) for $\bar{k} < 1$ and $\gamma < 0$ (stable) for $\bar{k} > 1$. By setting $\gamma = 0$ and neglecting terms of order $\bar{d}_e$, we find the marginal condition

$$0 = \frac{1}{\bar{k}_o} - \bar{k}_o,$$

and the marginal wavenumber $\bar{k}_o = 1$, recovering the previous result[1,2].

For the anisotropic case, the approximate dispersion relation is still given by Eq. (36) with $\alpha_j \neq 0$ in Λ [Eq. (30)]. As we can see from Eq. (30), the electron anisotropy effects are large because of the small gyroradius ($a_i^2/a_e^2 \propto m_i/m_e$, $\delta^2/a_e^2 >> 1$). As a result, it is likely that nonlinear effects become important for electrons on a time scale comparable to ω_{ci}^{-1}. This makes the present analysis unsuitable except for very small degrees of electron anisotropy, viz., $|T_{e\perp}/T_{e\parallel} - 1| << a_e/\delta$. Thus, in the remainder of this paper, we will primarily consider the case with anisotropic ions and isotropic electrons. Then, keeping only the leading terms, we have

$$\left(\Lambda \bar{d}_e\right)^2 \simeq 2\sqrt{\pi}\left(\frac{\delta}{a_e}\right)\left(1 + \frac{T_{i\perp}}{T_{e\perp}}\right)^{-1}\left(\frac{\gamma}{k v_{e\parallel}}\right) + 2\alpha_i \left(1 + \frac{T_{i\perp}}{T_{e\perp}}\right)^{-1}\left(\frac{\delta}{a_e}\right)\frac{m_e}{m_i}, \tag{38}$$

where $\alpha_i = \left(1 - T_{i\perp}/T_{i\parallel}\right)$. In marginal state, $\gamma = 0$ and

$$\left(\Lambda \bar{d}_e\right)^2 = 2\alpha_i\left(1 + \frac{T_{i\perp}}{T_{e\perp}}\right)^{-1}\left(\frac{\delta}{a_e}\right)\frac{m_e}{m_i}.$$

For systems in which (a_e/δ) and (m_e/m_i) are comparable such as the

magnetotail, $(\Lambda\bar{d}_e)^2 << 1$. Then, the marginal wavenumber $\bar{k}_o$ is given by

$$\frac{1}{\bar{k}_o} - \bar{k}_o = \sqrt{2}\ \alpha_i\left(1 + \frac{T_{i\perp}}{T_{e\perp}}\right)^{-1}\left(\frac{m_e}{m_i}\right)\left(\frac{\delta}{a_e}\right)^{3/2}. \tag{39}$$

Using Eqs. (38) and (39) in Eq. (36) and keeping only the leading terms, we find

$$\frac{\gamma}{kv_{e\parallel}} = \frac{1}{\sqrt{2\pi}}\left(\frac{a_e}{\delta}\right)^{3/2}\left(1 + \frac{T_{i\perp}}{T_{e\perp}}\right)\left[\left(\frac{1}{\bar{k}} - \bar{k}\right) - \sqrt{2}\ \alpha_i\left(1 + \frac{T_{i\perp}}{T_{e\perp}}\right)^{-1}\left(\frac{m_e}{m_i}\right)\left(\frac{\delta}{a_e}\right)^{3/2}\right]. \tag{40}$$

This is the approximate anisotropic dispersion relation obtained by matching the inner and asymptotic solutions at $z = d_e$. From Eq. (40), we find that the normalized growth rate γ/ω_{ci} has a maximum at

$$\bar{k}_c \equiv -\frac{1}{2}\left(\frac{1}{\bar{k}_o} - \bar{k}_o\right),$$

and

$$\left(\frac{\gamma}{\omega_{ci}}\right)_{max} = \frac{1}{\sqrt{2\pi}}\left(\frac{a_e}{\delta}\right)^{5/2}\left(\frac{m_i}{m_e}\right)\left(1 + \frac{T_{i\perp}}{T_{e\perp}}\right)\left(1 + \bar{k}_c^2\right). \tag{41}$$

Equation (36) is obtained to show the basic properties of the isotropic and anisotropic dispersion relations. One noteworthy property of this equation is that Λ is either purely real or purely imaginary. Using small-argument expansion of Z and W functions, it is easy to see that ω is nearly purely imaginary for the low-frequency perturbations being considered, as we assumed in the preceding discussion of approximate solutions. In the remainder of the paper, we specialize to the case of imaginary frequency with $\omega \equiv i\gamma$ so that $\gamma > 0$ corresponds to instability. The transcendental equation (36) has also been solved numerically to obtain the dispersion relation in detail. Figures 3 and 4 show the growth rate γ normalized to the asymptotic ion cyclotron frequency ω_{ci} versus the normalized $\bar{k} \equiv k\delta$. The dispersion curves are shown for several values of $T_{i\perp}/T_{i\parallel}$ and two values of (α_i/δ), 0.03 and

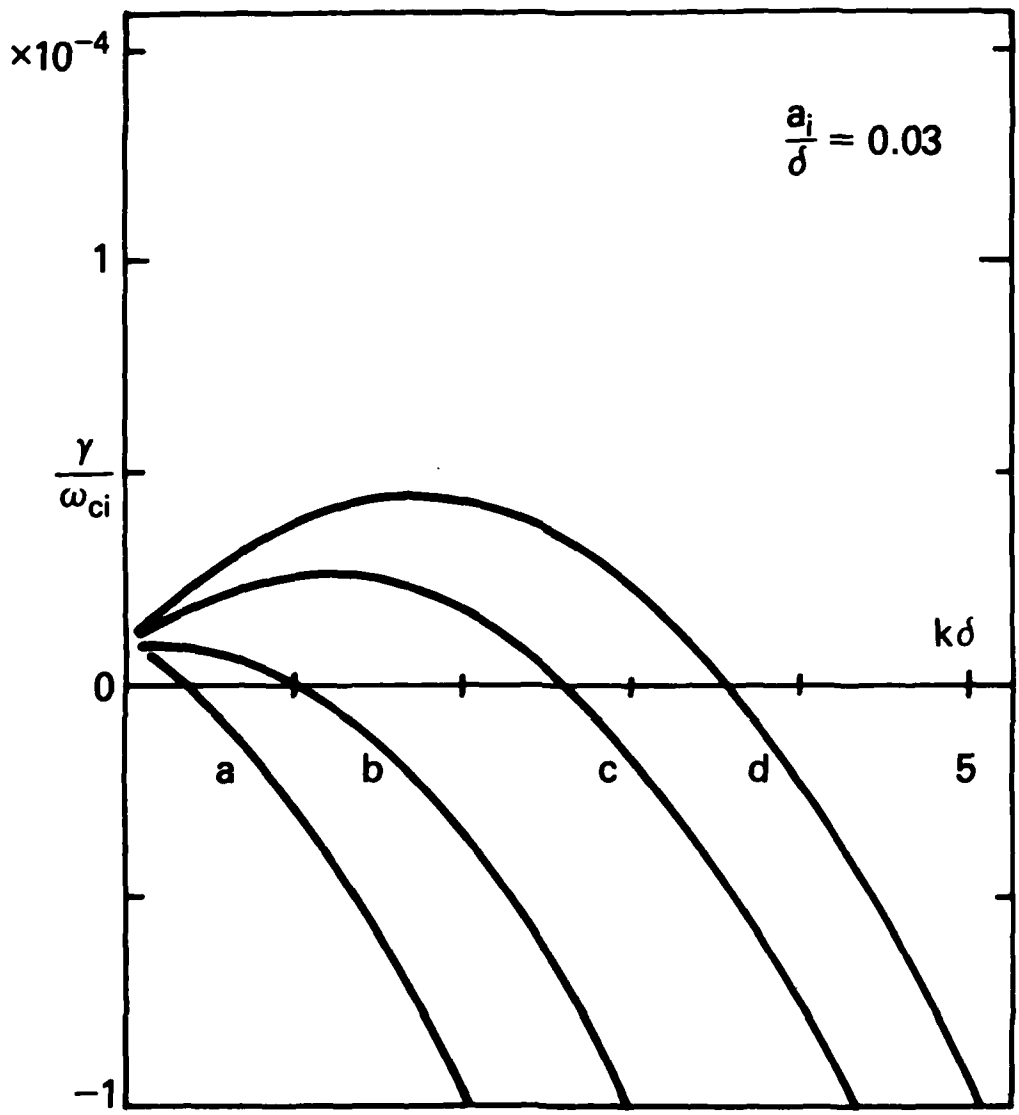

Fig. 3 Normalized growth rate (γ/ω_{ci}) versus $k\delta$ for $a_i/\delta = 0.03$ using the two-region approximation [Eq. (37)]. The value of $T_{i\perp}/T_{i\parallel}$ is (a) 0.9, (b) 1.0, (c) 1.1 and (d) 1.15. ($T_{e\perp}/T_{e\parallel} = 1$).

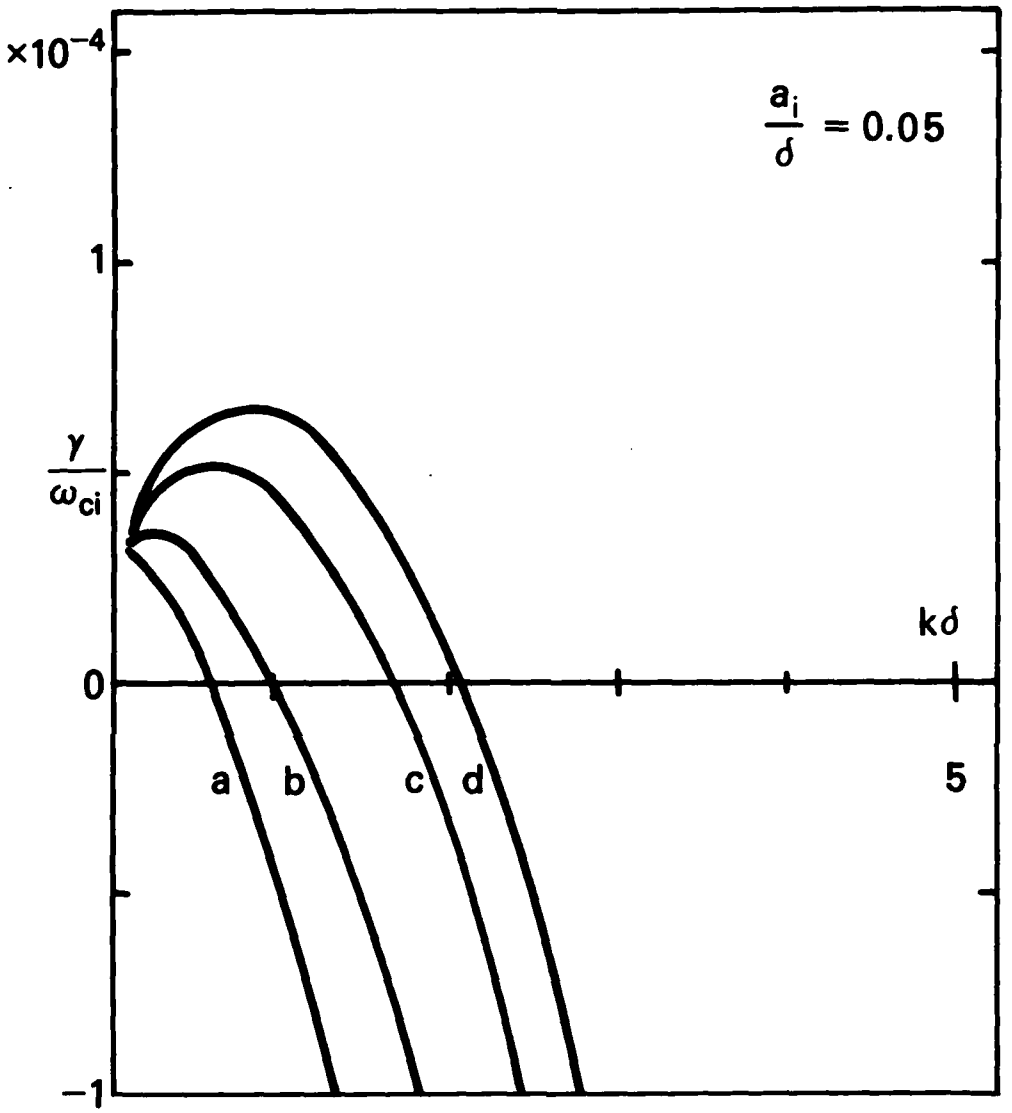

Fig. 4 Normalized growth rate (γ/ω_{ci}) versus $k\delta$ for $a_i/\delta = 0.05$ using Eq. (37). The value of $T_{i\perp}/T_{i\parallel}$ is (a) 0.9, (b) 1.0, (c) 1.1 and (d) 1.15. ($T_{e\perp}/T_{e\parallel} = 1$).

0.05. In particular, the value $a_i/\delta = 0.03$ roughly corresponds to the quiescent magnetotail parameters. In addition, we have used $T_{i\perp}/T_{e\perp} = 2$. In this case, $a_e/\delta \simeq 5 \times 10^{-4}$.

The curve b in each figure corresponds to the isotropic result[8] with the marginal wavenumber $k\delta = 1$ independently of (a_i/δ). Consistent with the previous conclusions[13], we find that temperature anisotropy with $T_{i\perp}/T_{i\parallel} > 1$ is destabilizing while anisotropy with $T_{i\perp}/T_{i\parallel} < 1$ is stabilizing. Here, $\underline{k}$ is parallel to $\underline{B}_o$ so that the case with the greater temperature perpendicular to $\underline{k}$ is more unstable. These figures also show that Eq. (39) describes the stability boundary accurately. For example, for $T_{i\perp}/T_{i\parallel} = 1.1$ and $a_i/\delta = 0.03$, we have $\bar{k}_o = 2.67$. For $a_i/\delta = 0.05$, we have $\bar{k}_o = 1.68$, in agreement with these figures. In addition, Eq. (40) is a good approximation for all the curves shown in these figures. In comparing Figs. 3 and 4, note that the two values of a_i/δ correspond to different values of δ and ω_{ci} so that γ and k are normalized to different scales [see Eqs. (14), (17) and (18)]. The curves are not completed for $k\delta \simeq 0$ because the theory breaks down as $k \to 0$. Comparing curves a, c and d with curve b in each of Figs. 3 and 4, we see that the effect of anisotropy is substantial. This is expected because the anisotropy term, the third term in Eq. (8), is greater than the isotropic term by a factor of $(kv_{j\parallel}/\omega) \gg 1$. In this regard, we point out that Laval and Pellat[12] used an energy method to show that the mode treated here is completely stabilized for

$$\frac{T_{e\perp}}{T_{e\parallel}} < 1 - \frac{a_e}{\delta} . \tag{42}$$

For the parameter used in Fig. 3, the right hand side is approximately 0.9995. Using this value of electron temperature anisotropy in Eq. (37), we find that the mode is in fact completely stabilized. With electron anisotropy, the square brackets in Eq. (40) would contain another term identical to the second term except for the replacement $e \to i$ and $m_e/m_i \to 1$. [See the discussion preceding Eq. (38)]. The reason for the extremely sensitive dependence on the electron anisotropy described above is that the electron term without the small mass ratio enhances the anisotropy effects discussed above. As a general remark, we note that γ/ω_{ci} is typically of the order of 10^{-4}. In addition, $\gamma/kv_{j\parallel}$ is also

of the order of 10^{-4} for the unstable parameter regimes for both species. Thus, the low frequency approximation used to derive Eq. (8) is justified a posteriori.

So far, we have examined anisotropic tearing-mode properties using the two-region matching method following a number of previous works. However, examination of Eq. (32) shows that, in the intermediate region, it is the ion orbits that dominate. Furthermore, because $d_i \gg d_e$, the effect of these ions is expected to be large. In order to study the anisotropic properties including the intermediate region, we have numerically integrated Eqs. (32) and (33) in regions II and III. The physically acceptable solution must have the asymptotic behavior given by Eq. (34) and the logarithmic derivative must be continuous at $z = d_i$ and $z = d_e$. At $z = d_e$, the derivative is matched to that of the analytic solution, Eq. (31). The matching condition then gives the linear anisotropic dispersion relation. The results are plotted in Figs. 5 and 6 for several values of $T_{i\perp}/T_{i\parallel}$ and for two values of a_i/δ, 0.03 and 0.05. Here, the electrons are isotropic.

Comparing Figs. (3) with (5) and (4) with (6), we see that inclusion of the ion orbits in the intermediate region modifies the growth rate and the stability boundary significantly. In general, the anisotropy effects are further enhanced by the inclusion of the intermediate region (region II). That is, for $T_{i\perp}/T_{i\parallel} < 1$, the mode is more strongly stabilized with the intermediate region than without it. For $T_{i\perp}/T_{i\parallel} > 1$, the instability is more strongly enhanced with the intermediate region than without it. However, the isotropic dispersion curves obtained using the "three-region" matching method are nearly identical to the corresponding ones obtained using the two-region approach. The absolute value of (γ/ω_{ci}) of curve b in Fig. 3 is greater than that of curve b in Fig. 5 by approximately 3% to 4% ($a_i/\delta = 0.03$). The absolute value of (γ/ω_{ci}) of curve b in Fig. 4 is also greater than that of curve b in Fig. 6 by similar amounts ($a_i/\delta = 0.05$). This agreement is nontrivial since Eq. (32) shows that the dominant ion orbits in the intermediate region modifies the eigenvalue equation significantly and indicates that the isotropic dispersion relation is indeed determined primarily by the resonant electrons in the inner region $|z| < d_e$. The above behavior can be

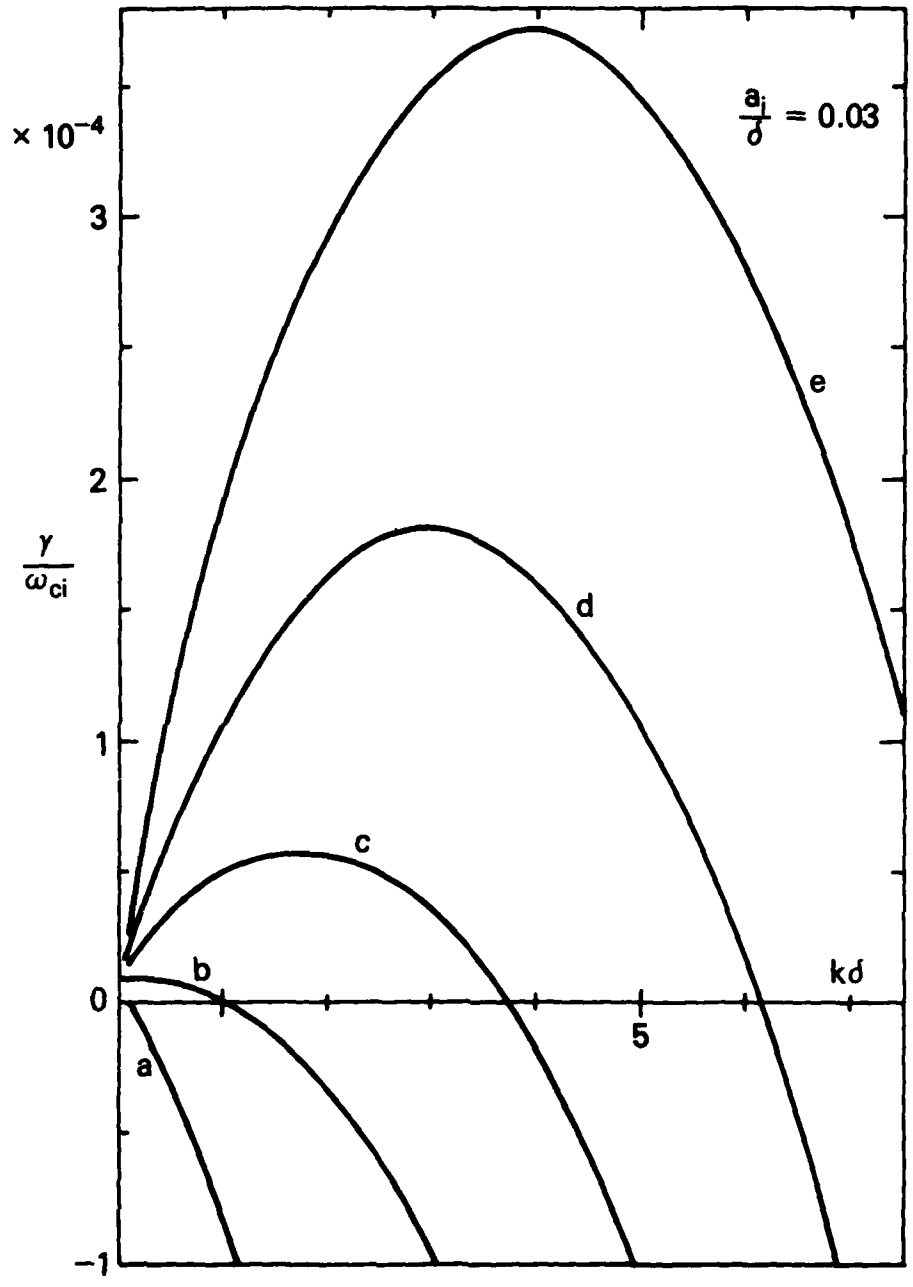

Fig. 5 Normalized growth rate (γ/ω_{ci}) versus $k\delta$ for $a_i/\delta = 0.03$ including the intermediate ion region. The value of $T_{i\perp}/T_{i\parallel}$ is (a) 0.9, (b) 1.0, (c) 1.05, (d) 1.1 and (e) 1.15. ($T_{e\perp}/T_{e\parallel} = 1$).

understood from Eqs. (6) or (8) by noting that $ikqS_y$ is the time-integrated Lorentz force in the x-direction causing the particles to bunch. Since the ion orbits are larger than the electron orbits by approximately $d_i/d_e \simeq 4$, the accumulated influence is also increased. It is evident that the Lorentz force term is zero in the isotropic case. It is of interest to note that the force responsible for the anisotropic effects is similar to that in the mirror instability[20]. However, unlike the mirror instability, there is no threshold value of $T_{i\perp}/T_{i\parallel}$ that is required for the onset of the anisotropic effects.

Figures 5 and 6 show that for $T_{i\perp}/T_{i\parallel} > 1$ the maximum growth rate is enhanced by one order of magnitude or more from the isotropic case and that the marginal wavenumber is increased. For $T_{i\perp}/T_{i\parallel} < 1$, the instability is essentially stabilized. Note that, as before, (γ/ω_{ci}) is typically of the order of 10^{-4} so that the low frequency approximation is justified. The results are shown for $T_{i\perp}/T_{i\parallel}$ up to 1.15. For higher $(T_{i\perp}/T_{i\parallel} \gtrsim 1.3)$ degrees of anisotropy, the increasing value of (γ/ω_{ci}) would render the low frequency and constant-ψ approximations invalid. The dashed line (e) in Fig. 6 shows the dispersion curve for $T_{i\perp}/T_{i\parallel} = 1.1$ with the $\underline{\nabla B}$ contribution neglected. We see that the qualitative behavior is not significantly changed and that the $\underline{\nabla B}$ drift has the opposite, albeit small, effect from the axis-crossing orbits. This is easy to understand since the guiding center of a drifting particle is opposite to the mean drift velocity of the plasma layer [Eq. (25)].

Figure 7 shows the maximum growth rate $(\gamma/\omega_{ci})_{max}$ as a function of temperature anisotropy $(T_{i\perp}/T_{i\parallel})$. In Fig. 8, we have plotted the eigenfunction $\hat{\psi}(z)$ for $|z| > d_e$ for two values of $T_{i\perp}/T_{i\parallel}$. Both curves correspond to the respective maximum growth rates $(\gamma/\omega_{ci})_{max}$. The matching surfaces at $|z| = d_e$ and $|z| = d_i$ are also shown. We see that the constant-ψ approximation is reasonable for the values of $T_{i\perp}/T_{i\parallel}$ used here. However, for $T_{i\perp}/T_{i\parallel} \gtrsim 1.3$, the variation in $\hat{\psi}$ within the ion layer becomes substantially greater.

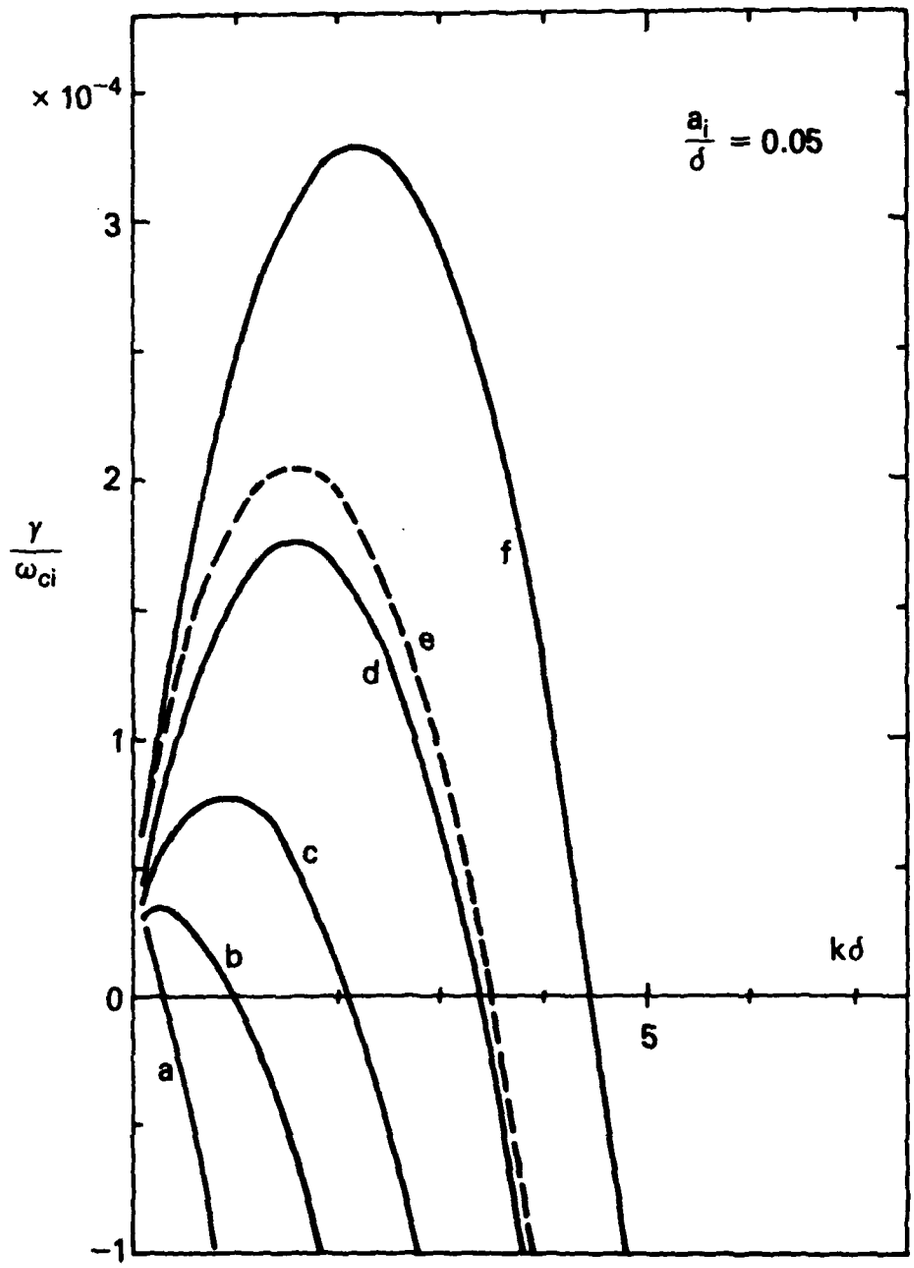

Fig. 6 Normalized growth rate (γ/ω_{ci}) versus $k\delta$ for $a_i/\delta = 0.05$ including the intermediate ion region. The value of $T_{i\perp}/T_{i\parallel}$ is (a) 0.9, (b) 1.0, (c) 1.05, (d) 1.1, (e) 1.1 with ∇B neglected and (f) 1.15. ($T_{e\perp}/T_{e\parallel} = 1$).

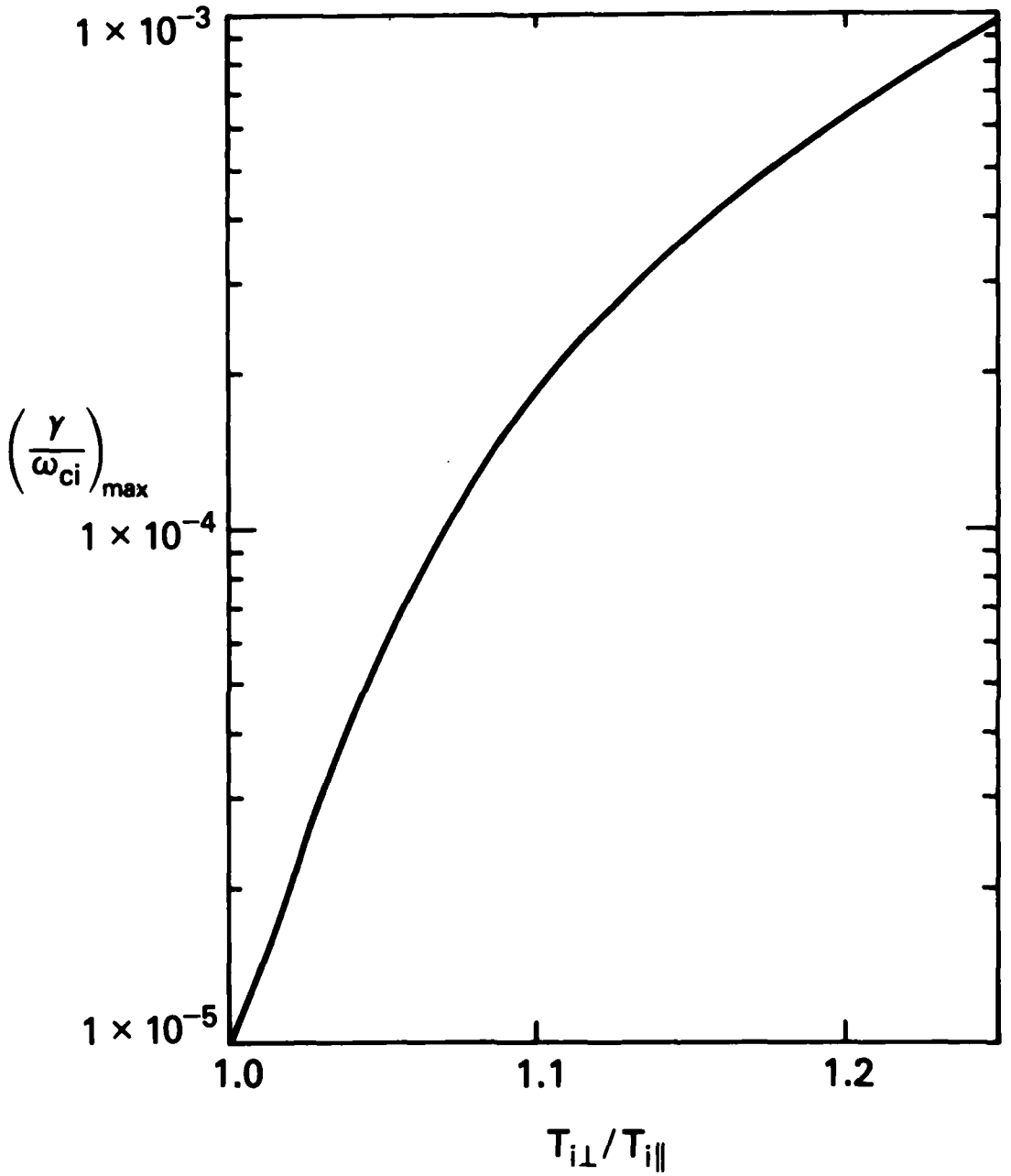

Fig. 7 Maximum growth rate $(\gamma/\omega_{ci})_{max}$ versus $T_{i\perp}/T_{i\parallel}$ for $a_i/\delta = 0.03$ and $T_{e\perp}/T_{e\parallel} = 1$.

IV. SUMMARY

In this paper, we have investigated the collisionless tearing-mode properties of an anisotropic ($T_\perp \neq T_\parallel$) neutral sheet. Both ions and electrons are described by Vlasov distribution functions. Using simplified particle orbits and constant-ψ approximation, the perturbed distribution function is evaluated for low frequency perturbations ($\gamma/\omega_{ci} \ll 1$) with $\underline{k} \parallel \underline{B}_o$. The first-order current densities are explicitly found [Eqs. (22), (23), (27) and (28)] and eigenvalue equation is obtained for the three regions [Fig. 2 and Eqs. (29), (32) and (33)]. The equation is solved using both analytic approximations and numerical methods to obtain the linear dispersion relation (Figs. 3, 4, 5 and 6) and the eigenmode structure (Fig. 8). First, by neglecting the ion intermediate region (region II), the conventional two-region matching method is used to find the approximate anisotropic dispersion relation [Eq. (40) and Figs. 3 and 4] as well as other dispersion properties [Eqs. (39) and (41)]. Then, the full eigenvalue equation is numerically integrated in regions II and III. The three-region matching condition then gives rise to the anisotropic dispersion relation illustrated in Figs. 5 and 6 for a number of parameter values. It is shown that temperature anisotropy with $T_{i\perp}/T_{i\parallel} > 1$ enhances the growth rate by as much as an order of magnitude or more while anisotropy with $T_{i\perp}/T_{i\parallel} < 1$ strongly stabilizes the mode. This is consistent with previous results based on energy principle[12] and marginal stability[13] calculations. It is also found that the conventional approach of matching the inner and outer solutions at the electron inner region ($|z| < d_e$) is not adequate in the anisotropic case. An intermediate region ($d_e < |z| < d_i$) is identified in which the axis-crossing ion orbits are dominant. It is the ions in this region that account for the substantial differences as exhibited by Figs. 3, 4, 5 and 6. The use of simplified orbits also allows evaluation of the effects of different orbits explicitly. In particular, it is found that the inner orbits and outer orbits (the ∇B drift orbits) have the opposite effects on the growth rate: where the inner orbits are destabilizing, the outer orbits are stabilizing and vice versa in the anisotropic case.

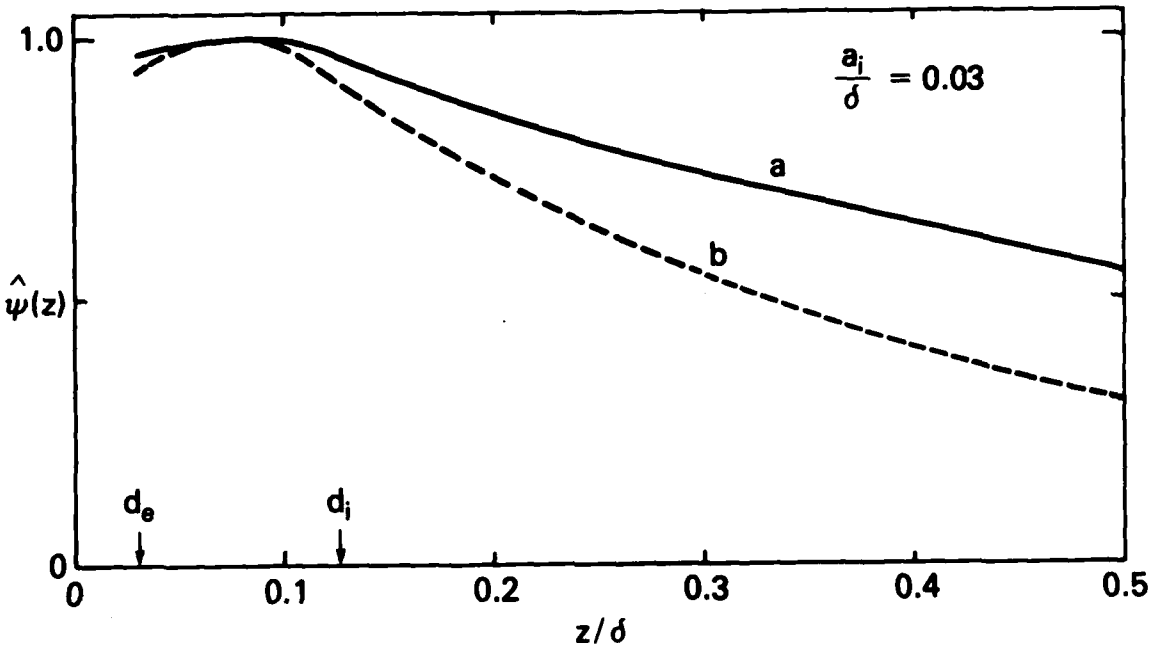

Fig. 8 Eigenfunction $\hat{\psi}(z)$ versus z/δ corresponding to $(\gamma/\omega_{ci})_{max}$ for (a) $T_{i\perp}/T_{i\parallel} = 1.05$ and (b) $T_{i\perp}/T_{i\parallel} = 1.1$. $a_i/\delta = 0.03$. The matching boundaries are indicated: $|\bar{z}| = d_e$ and $|\bar{z}| = d_i$. $(T_{e\perp}/T_{e\parallel} = 1)$.

A physical system for which the present analysis may be applicable is the earth's magnetotail. The previous works on the tearing-mode stability of such a system have studied isotropic neutral sheets (see, for example, Refs. 8, 10 and 11). In light of the fact that the magnetotail is highly collisionless, it is reasonable to expect the temperature distribution to be generally anisotropic. Our present results suggest that the linear tearing-mode properties of the magnetotail and similar physical systems are dominated by the anisotropic tearing-mode. In fact, the $\underline{k} \parallel \underline{B}_o$ mode can grow significantly faster than previously predicted if temperature anisotropy is present ($\alpha_i > a_i/\delta$). Thus, the particle temperature distribution is a critically important quantity for understanding the linear tearing-mode stability properties.

The present analysis utilized simple approximate orbits in evaluating the orbit integrals. In the isotropic case, the two-region approach[8] yielded results in agreement with numerical results,[4] indicating that the stability properties are not critically dependent on the precise orbits. In the anisotropic case, however, the large ion orbits are important so that a more accurate calculation of the orbit integrals is desirable. In the present analysis, the orbits that are neglected are mainly those of particles with energy substantially greater than the typical velocities, constituting a relatively small fraction of the total particles. In conjunction with the fact that the low frequency and constant-ψ approximations are well satisfied by the results, we expect the present results to be a good first approximation for understanding the essential physics of the collisionless anisotropic tearing-mode properties.

Acknowledgments

We are grateful to Drs. J. F. Drake, J. M. Finn, and Y. C. Lee for insightful discussions. This research was supported by NASA W-14365 and ONR.

References

1. H. P. Furth, Nucl. Fusion Suppl. Pt. 1, 169 (1962).
2. D. Pfirsch, Z. Naturforsch. 17a, 861 (1962).
3. G. Laval and R. Pellat, Compt. Reud. 259, 1706 (1964).
4. F. C. Hoh, Phys. Fluids 9, 277 (1966).
5. G. Laval, R. Pellat, and M. Vuillemin, in Plasma Physics and Controlled Nuclear Fusion Research (International Atomic Energy Agency, Vienna, 1966), 2, 259.
6. K. Schindler, in Proceedings of the Seventh International Conference on Phenomena in Ionized Gases (Gradevinska Knjiga, Beograd, Yugoslavia, 1966), Vol. II, 736.
7. K. Schindler and M. Soop, Phys. Fluids 11, 1192 (1968).
8. M. Dobrowolny, Nuovo Cimento B 55, 427 (1968).
9. N. F. Ness, J. Geophys. Res. 70,2989 (1965).
10. B. Coppi, G. Laval, and R. Pellat, Phys. Rev. Lett. 16, 1207 (1966).
11. K. Quest and F. V. Coroniti, J. Geophys. Res. 86, 3299 (1981).
12. G. Laval and R. Pellat, ESRO SP-36, 5 (1968).
13. J. Chen and R. C. Davidson, Phys. Fluids 24, 2208 (1981).
14. B. Basu and B. Coppi, Phys. Rev. Lett. 48, 799 (1982).
15. B. U. Ö. Sonnerup, J. Geophys. Res. 76, 8211 (1971).
16. J. P. Holdren, Ph.D. thesis, Stanford University IPR Report No.351 (1970)
17. E. G. Harris, Nuovo Cimento 23, (1962).
18. J. F. Drake and Y. C. Lee, Phys. Fluids 20, 1341 (1977).
19. A. A. Galeev and L. M. Zelenyi, Sov. Phys. JETP 42, 450 (1975).
20. *This form of solution was pointed out to us by J. M. Finn.*
21. See, for example, G. Schmidt, Physics of High Temperature Plasmas, 2nd ed., Academic Press, New York (1979).

DISTRIBUTION LIST

Director
Naval Research Laboratory
Washington, D.C. 20375
ATTN: Code 4700 (26 Copies)
Code 4701
Code 4780 (100 copies)
Code 4187 (E. Szuszczewicz)
Code 4187 (P. Rodriguez)
Code 2628 20 copies

University of Alaska
Geophysical Institute
Fairbanks, Alaska 99701
ATTN: Library
S. Akasofu
J. Kan
J. Roederer
L. Lee

University of Arizona
Dept. of Planetary Sciences
Tucson, Arizona 85721
ATTN: J.R. Jokipii

University of California, S.D.
LaJolla, California 92037
(Physics Dept.):
ATTN: J.A. Fejer
T. O'Neil
J. Winfrey
Library
J. Malmberg
(Dept. of Applied Sciences):
ATTN: H. Booker

University of California
Los Angeles, California 90024
(Physic Dept.):
ATTN: J.M. Dawson
B. Fried
J.G. Moralles
W. Gekelman
R. Stenzel
Y. Lee
A. Wong
F. Chen
M. Ashour-Abdalla
Library
J.M. Cornwall

(Institute of Geophysics and
Planetary Physics):
ATTN: Library
C. Kennel
F. Coroniti

Columbia University
New York, New York 10027
ATTN: R. Taussig
R.A. Gross

University of California
Berkeley, California 94720
(Space Sciences Laboratory):
ATTN: Library
M. Hudson
(Physics Dept.):
ATTN: Library
A. Kaufman
C. McKee
(Electrical Engineering Dept.):
ATTN: C.K. Birdsall

University of California
Physics Department
Irvine, California 92664
ATTN: Library
G. Benford
N. Rostoker
C. Robertson
N. Rynn

California Institute of Technology
Pasadena, California 91109
ATTN: R. Gould
L. Davis, Jr.
P. Coleman

University of Chicago
Encrico Fermi Institute
Chicago, Illinois 60637
ATTN: E.N. Parker
I. Lerche
Library

University of Colorado
Dept. of Astro-Geophysics
Boulder, Colorado 80302
ATTN: M. Goldman
Library

Cornell University
School of Applied and Engineering Physics
College of Engineering
Ithaca, New York 14853
ATTN: Library
R. Sudan
B. Kusse
H. Fleischmann
C. Wharton
F. Morse
R. Lovelace

Harvard University
Cambridge, Massachusetts 02138
ATTN: Harvard College Observatory
(Library)
G.S. Vaina
M. Rosenberg

Harvard University
Center for Astrophysics
60 Garden Street
Cambridge, Massachusetts 02138
ATTN: G.B. Field

University of Iowa
Iowa City, Iowa 52240
ATTN: C.K. Goertz
D. Gurnett
G. Knorr
D. Nicholson

University of Houston
Houston, Texas 77004
ATTN: Library

University of Maryland
Physics Dept.
College Park, Maryland 20742
ATTN: K. Papadopoulos
H. Rowland
C. Wu

University of Michigan
Ann Arbor, Michigan 48140
ATTN: E. Fontheim

University of Minnesota
School of Physics
Minneapolis, Minnesota 55455
ATTN: Library
J.R. Winckler
P. Kellogg

M.I.T.
Cambridge, Massachusetts 02139
ATTN: Library
(Physics Dept.):
ATTN: B. Coppi
V. George
G. Bekefi
T. Dupree
R. Davidson
(Elect. Engineering Dept.):
ATTN: R. Parker
A. Bers
L. Smullin
(R.L.E.):
ATTN: Library
(Space Science):
ATTN: Reading Room

Princeton University
Princeton, New Jersey 08540
Attn: Physics Library
Plasma Physics Lab. Library
C. Oberman
F. Perkins
T.K. Chu
H. Okuda
V. Aranasalan
H. Hendel
R. White
R. Kurlsrud
H. Furth
S. Yoshikawa
P. Rutherford

Rice University
Houston, Texas 77001
Attn: Space Science Library
R. Wolf

University of Rochester
Rochester, New York 14627
ATTN: A. Simon

Stanford University
Institute for Plasma Research
Stanford, California 94305
ATTN: Library

Stevens Institute of Technology
Hoboken, New Jersey 07030
ATTN: B. Rosen
G. Schmidt
M. Seidl

University of Texas
Austin, Texas 78712
ATTN: W. Drummond
V. Wong
D. Ross
W. Horton
D. Choi
R. Richardson
G. Leifeste

College of William and Mary
Williamsburg, Virginia 23185
Attn: F. Crownfield

Lawrence Livermore Laboratory
University of California
Livermore, California 94551
ATTN: Library
B. Kruer
J. Thomson
J. Nucholls
J. DeGroot
L. Wood
J. Emmett
B. Lasinsky
B. Langdon
R. Briggs
D. Pearlstein

Los Alamos National Laboratory
P.O. Box 1663
Los Alamos, New Mexico 87545
ATTN: Library
D. Forslund
J. Kindel
B. Bezzerides
H. Dreicer
J. Ingraham
R. Boyer
C. Nielson
E. Lindman
L. Thode

N.O.A.A.
325 Broadway S.
Boulder, Colorado 80302
ATTN: J. Weinstock
Thomas Moore (SEL, R-43)
W. Bernstein
D. Williams

Sandia Laboratories
Albuquerque, New Mexico 87115
ATTN: A. Toepfer
G. Yeonas
D. VanDevender
J. Freeman
T. Wright

Bell Laboratories
Murray Hill, New Jersey 07974
ATTN: A. Hasegawa

Lockheed Research Laboratory
Palo Alto, California 94304
ATTN: M. Walt
J. Cladis

Physics International Co.
2400 Merced Street
San Leandro, California 94577
ATTN: J. Benford
S. Putnam
S. Stalings
T. Young

Science Applications, Inc.
Lab. of Applied Plasma Studeis
P.O. Box 2351
LaJolla, California 92037
ATTN: L. Linson
J. McBride

Goddard Space Flight Center
Greenbelt, Maryland 20771
ATTN: M. Goldstein
T. Northrop
T. Birmingham

TRW Systems Group
Space Science Dept.
One Space Park
Redondo Beach, California 90278
ATTN: R. Fredericks
F. Scarf

National Science Foundation
Atmospheric Research Section (ST)
Washington, D.C. 20550
ATTN: D. Peacock

Goddard Space Flight Center
Code 620
Greenbelt, Maryland 20771
ATTN: Robert F. Benson

NASA Headquarters
Code EE-8
Washington, D.C. 20546
ATTN: Dr. I. Schmerling
Dr. J. Lynch
Dr. D. Butler

Klumpar, David
Center for Space Sciences
P.O. Box 688
University of Texas
Richardson, Texas 75080

Leung, Philip
Dept. of Physics
University of California
405 Hilgard Avenue
Los Angeles, California 90024

Lysak, Robert
School of Physics and Astronomy
University of Minnesota
Minneapolis, MN 55455

Schulz, Michael
Aerospace Corp.
A6/2451, P.O. Box 92957
Los Angeles, California 90009

Shawhan, Stanley
Dept. of Physics & Astronomy
University of Iowa
Iowa City, Iowa 52242

Temerin, Michael
Space Science Lab.
University of California
Berkeley, California 94720

Vlahos, Loukas
Dept. of Physics
University of Maryland
College Park, Maryland 20742

Matthews, David
IPST
University of Maryland
College Park, Maryland 20742

Schunk, Robert W.
Utah State University
Dept. of Physics
Logan, Utah 84322

Defense Technical Information Center
Cameron Station
5010 Duke Street
Alexandria, VA 22314 (2 copies)


ATE
LME